Characteristics of Spinel Inclusions Formed After Reoxidation of Calcium-Treated Aluminum-Killed Steel

A thermodynamic model was developed and a laboratory vacuum induction furnace was employed to simulate the reoxidation of aluminum-killed calcium-treated steels. A method for representing the size distribution of inclusions using the population density function was applied to study the effect of reoxidation on the inclusion characteristics. A comparison of the size distributions of spinel inclusion populations showed that spinel inclusions produced after reoxidation are larger than those formed prior to reoxidation and calcium treatment.

Authors

Obinna Adaba
Ph.D. candidate, Missouri University of Science and Technology, Rolla, Mo., USA
omakc2@mst.edu

Pallava Kaushik
lead researcher, ArcelorMittal Global R&D – East Chicago, East Chicago, Ind., USA
pallava.kaushik@arcelormittal.com

Ronald J. O'Malley
F. Kenneth Iverson Chair for Steelmaking Technology, director, Kent D. Peaslee Steel Manufacturing Research Center, and professor of metallurgy, Missouri University of Science and Technology, Rolla, Mo., USA
omalleyr@mst.edu

Simon N. Lekakh
research professor, Missouri University of Science and Technology, Rolla, Mo., USA
lekakhs@mst.edu

Von L. Richards
professor emeritus, Missouri University of Science and Technology, Rolla, Mo., USA
vonlr@mst.edu

Erik Mantel
ArcelorMittal Global R&D – East Chicago, East Chicago, Ind., USA

Randy Hall
ArcelorMittal Global R&D – East Chicago, East Chicago, Ind., USA

Eric J. Ellis
ArcelorMittal Global R&D – East Chicago, East Chicago, Ind., USA

Reoxidation of liquid steel during the last stages of steel production affects the inclusion characteristics and is harmful to process stability, mechanical properties, and the overall quality of the cast product.[1] In aluminum-killed steels, alumina inclusions produced after liquid steel deoxidation clog submerged-entry nozzles (SEN) and their irregular shape acts as preferential sites for crack initiation. To prevent these harmful effects, calcium is typically added at the end of ladle metallurgy to modify them to liquid spherical calcium aluminates. Liquid steel reoxidation produces new alumina inclusions that, in the absence of calcium, retain their harmful qualities and negate the benefit of calcium treatment. In steels with sufficient magnesium in solution, spinel inclusions can also be formed after reoxidation.[1,2] These inclusions have been observed to cause hook cracks in line pipe steels.[3] The objective of this research was to investigate the formation and characteristics of spinel inclusions after liquid steel reoxidation.

Formation of Spinels in Ca-treated Reoxidized Steel — Results from studies conducted in two industrial mini-mills showed ladle slag as the source of magnesium for spinel formation in liquid steel.[3] Spinel inclusions were observed after the desulfurization process where the steel was continuously mixed with the MgO-saturated slag using argon gas. Eqs. 1 and 2 describe the two-step mechanism for the formation of spinels in liquid steel. At the end of the ladle metallurgy process, the spinel inclusions were modified by calcium to liquid calcium-magnesium aluminates. As mentioned earlier, these modified inclusions are less harmful to the casting process and steel properties. Also observed was the formation of CaS inclusions that resulted from overtreatment. The reaction mechanism for the calcium modification of spinels is given by Eq. 3 and shows the possibility of magnesium re-dissolution into steel.

$$3(MgO) + 2[Al] = 3[Mg] + (Al_2O_3) \quad \text{(Eq. 1)}$$

$$[Mg] + 2[Al] + 4[O] = (MgO \cdot Al_2O_3) \quad \text{(Eq. 2)}$$

$$[Ca] + (MgAl_2O_4) = CaO \cdot Al_2O_3 + [Mg] \quad \text{(Eq. 3)}$$

Thermodynamic calculations using commercial software allows for consideration of complex reactions involving the formation of oxide and sulfide inclusions. In such simulations, several assumptions can be made. For example, calculations can be done with additions into a closed system, or into a partially open system by removing selected reaction products. Calculations were done using Factsage 6.4 to simulate both the calcium modification process and the effect of liquid steel reoxidation on the change in the inclusion composition. Using a typical line pipe steel composition, these calculations were done at a temperature and pressure of 1,600°C and

This article is available online at AIST.org for 30 days following publication.

Figure 1

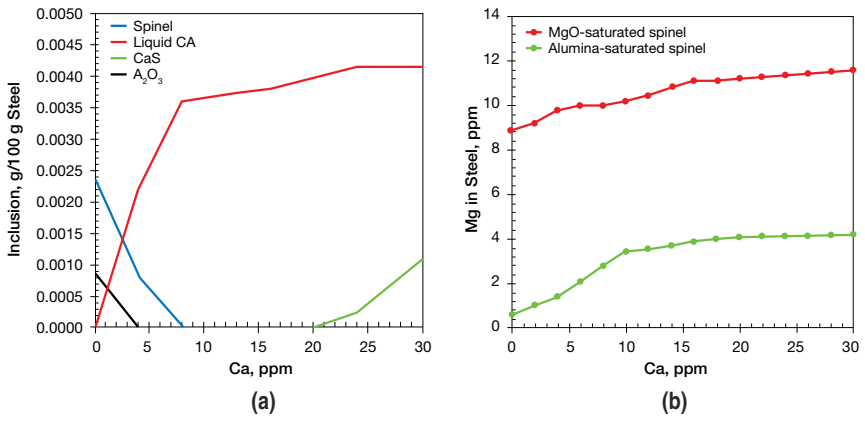

Thermodynamic simulation of spinel modification by calcium using Factsage v6.4. Target liquid inclusions form between 10 to 20 ppm Ca. Dissolved magnesium also increases during the process.

1 atm, respectively. Fig. 1a shows the results of the calcium modification process in a closed liquid steel system. Calcium in the range of 10 to 20 ppm results in fully modified liquid calcium-magnesium-aluminate inclusions. At higher levels of calcium (>25 ppm), solid CaS inclusions are formed for similar sulfur content of 30 ppm in steel. During the calcium modification process, the dissolved magnesium content in the liquid steel increased from less than 1 ppm to about 4 ppm (Fig. 1b). This calculation was done for an alumina-saturated spinel. Also shown in Fig. 1b is the calculated increase in dissolved magnesium during modification of an MgO-saturated spinel inclusion. At steelmaking temperatures, pure spinel is stable over a range of MgO contents. The MgO content in spinel varies from 20 to 30%. For an MgO-saturated spinel (about 30% MgO), the dissolved magnesium content after spinel modification by calcium is as high as 12 ppm.

Reoxidation of Ca-treated liquid steel during transfer of steel from the ladle and into tundish and mold has been observed in industrial practice, which decreases the benefits of the calcium treatment. To study the effect of reoxidation on the inclusions, calculations were done for an initial 21-ppm calcium-treated steel with different added amounts of oxygen. The result of this calculation is shown in Fig. 2. After reoxidation with 30 ppm oxygen, the calculation indicates the re-formation of spinel and solid calcium-aluminate inclusions in the liquid steel. With increased oxygen content, these inclusions transform to more complex solid calcium-magnesium aluminates. The results from this thermodynamic study clearly indicate that:

1. Calcium reacts with MgO in spinel and in conditions where Mg vaporization is suppressed, magnesium dissolves in liquid steel. This is in agreement with literature.[2]
2. Liquid steel reoxidation after calcium treatment can produce newly formed spinel inclusions when there is sufficient magnesium in solution.

To verify these results, and also to compare the spinel inclusion size and shape formed after reoxidation with those observed before reoxidation, laboratory experiments were performed and samples for inclusion analysis collected. To represent the size distribution of the inclusions, the method of population density function (PDF) was applied.

Size Distribution of Inclusions — Reoxidation of liquid steel produces new inclusions and can be observed from the shape change of the inclusion size distribution.[4] The size distribution of particles can be described by either log-normal or fractal distributions, depending on the chemical and physical processes occurring in the liquid steel.[4,5] These distributions are described by Eqs. 4 and 5, respectively, where $f(x)$ is the frequency of inclusions in a given size bin or population density function (PDF), and "x" is the inclusion diameter. "α" and "β" are constants related to the mean and shape of the log normal distribution, and "C" and "D" are constants of the fractal distribution. In an ln-ln plot of the PDF and inclusions diameter, the shape of the PDF is either quadratic or linear as shown by Eqs. 6 and 7, respectively.

$$f(x)=\left[\frac{1}{x\beta\sqrt{2\pi}}\right]\exp\left[-\left(\frac{1}{2\beta^2}\right)\left(\ln x-\alpha^2\right)\right] \quad \text{(Eq. 4)}$$

$$f(x)=\frac{C}{x^D} \quad \text{(Eq. 5)}$$

$$\ln\left(f(x)\right)=\frac{-(\ln x)^2}{2\beta^2}+\left(\frac{\alpha-\beta^2}{\beta^2}\right)(\ln x)+\ln\left(\frac{1}{\beta\sqrt{2\pi}}\right)-\frac{1}{2\beta^2}\alpha^2 \quad \text{(Eq. 6)}$$

Figure 2

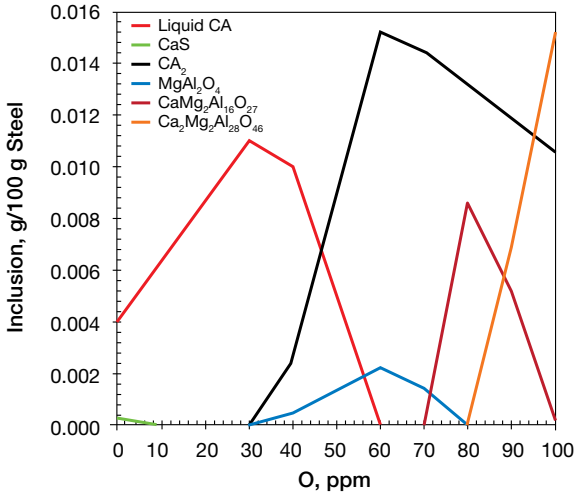

Thermodynamic simulation of the inclusion evolution in reoxidized calcium-treated steel. Newly formed spinel inclusions are observed in steel reoxidized with 30 ppm oxygen.

$$\ln(f(x)) = \ln(C) - D\ln(x) \quad \text{(Eq. 7)}$$

Different methods have been applied to interpret the size distribution of particles[6] and understand the conditions that produce the different shapes. The concept of population balance was first introduced and developed by Randolph and Larson in the field of chemical engineering and later applied to rocks by Marsh.[7,8] This method is based on a population balance of a number of particles in a given size range. By making assumptions of continuous nucleation and size-independent growth rate for crystal rocks, a plot of the log of the frequency and size produced a linear distribution. Cashman et al.,[8] however, also observed quadratic distributions in some systems and proposed Ostwald ripening as the cause for the shape change. Fig. 3 shows the proposed mechanism for the different shape distributions by Cashman.

Figure 3

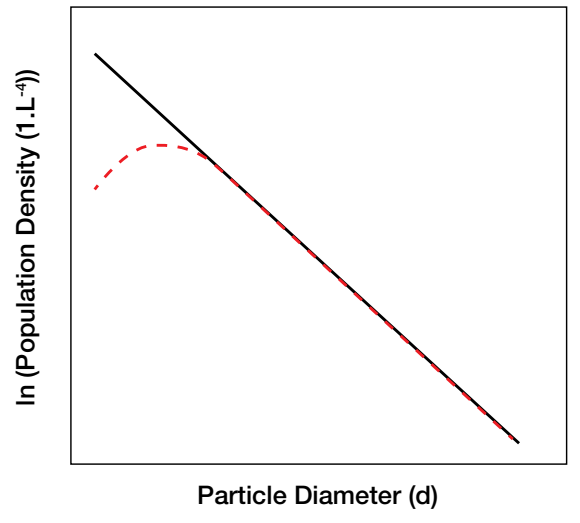

Particle distributions and the mechanism of formation. Mechanism proposed by Marsh. Distribution starts as linear and transforms to quadratic shape due to Ostwald ripening.

Due to failure of the population balance technique to successfully model the shape for many crystal systems in nature and from observations that most crystal size distributions are lognormal, Eberl et al.[6] simulated the growth of crystals under different conditions by numerical methods. Based on values of "β" and "α," growth mechanisms for different crystal size distribution (CSD) shapes were proposed. Table 1 is a summary of the proposed growth mechanisms under different conditions. This method was applied by E. Zinngrebe et al.,[4] and from their studies, quadratic inclusion size distributions observed after aluminum deoxidation was transformed to linear at the end of the LMF treatment. They proposed this linear distribution as a result of conditions of kinetic equilibrium between the liquid steel and inclusions.

The CSD method was applied to lollipop samples taken during a start-up heat to understand the conditions that produce each shape distribution. The samples were taken from an industrial mini-mill during liquid steel processing and are different from the laboratory samples. For a start-up heat, reoxidation has been observed to occur during liquid steel transfer from the ladle to the tundish. This is because the liquid steel is totally exposed to the atmosphere at the start of transfer until a sufficient amount of steel has been transferred into the tundish and after which slag additions are made.

Results and Discussions

Laboratory Experiments and Sample Analysis — To verify the formation of spinels after reoxidation, laboratory experiments were carried out in a 45-kg vacuum induction furnace. Three heats with changes in the alloy and the sequence of alloy additions after calcium treatments were performed. Fig. 4 is a schematic of the three heats and the respective additions. After melting and before alloy additions, air was removed from the chamber and filled with argon gas to 0.7 atm. Oxygen in the form of Fe_2O_3 was added for reoxidation while magnesium and calcium were added in the form of magnesium alloy and calcium silicon wire (CaSi) for spinel formation and calcium treatment, respectively. Immersion lollipop samples were taken

Table 1

Proposed Growth Mechanisms for Different CSD Shapes

System	Growth mechanism	CSD shape	Comments
Open	Nucleation and growth with constant or accelerating nucleation rate	Asymptotic	β^2 increases exponentially with increase in α
	Nucleation and growth with decaying nucleation rate	Lognormal	β^2 increases linearly with increase in α
	Surface-controlled growth	Lognormal	β^2 increases linearly with increase in α
	Supply-controlled growth	Preserves shape of previous CSD	β^2 remains constant with increase in α; therefore, steady-state reduced profiles
Closed	Ostwald ripening (supply-controlled)	CSD becomes more symmetrical with increasing percentage of ripening, becomes negatively skewed, and eventually approaches universal steady-state reduced profile	Distribution maximum moves to the right of theoretical lognormal curve. Generally, β^2 decreases with increase in α. Universal steady-state profile may not be reached.
	Random ripening (supply-controlled). Also termed non-Ostwald or kinetic ripening.	Preserves shape of previous CSD	A large amount of material passes through solution for a small increase in mean size. β^2 remains constant with increase in α; therefore steady-state reduced profiles.
	Agglomeration	Can be pseudo-lognormal or multimodal, or have other shapes	Very little material need pass through solution for a large increase in mean size. If most of the crystals are involved, β^2 may decrease; otherwise, it may increase.

Figure 4

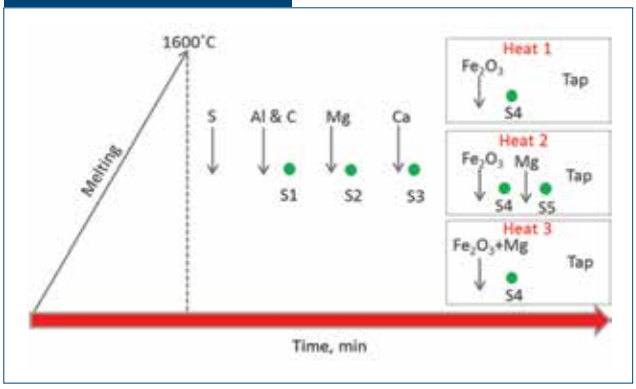

Schematic of the three heats and the respective alloying and sampling schedule.

from the liquid steel after respective additions. At the end of the experiment, the liquid steel was poured into a slab 12 inches long, 9 inches wide and 3 inches thick. Samples were also taken from the slab and analyzed.

Analysis of Lollipop Samples: Collected lollipop samples were analyzed for liquid steel composition and nonmetallic inclusions. To determine the magnesium content, induction-coupled plasma (ICP) was used, while a spark emission spectrometer was used for other elements. After chemical analysis, samples were sectioned, polished and analyzed for inclusions using automated scanning electron microscopy/energy-dispersive x-ray spectroscopy (SEM/EDS). A scan area of 100 mm^2 was considered for all lollipop samples and a minimum inclusion size of 1µm was selected.

Figure 5

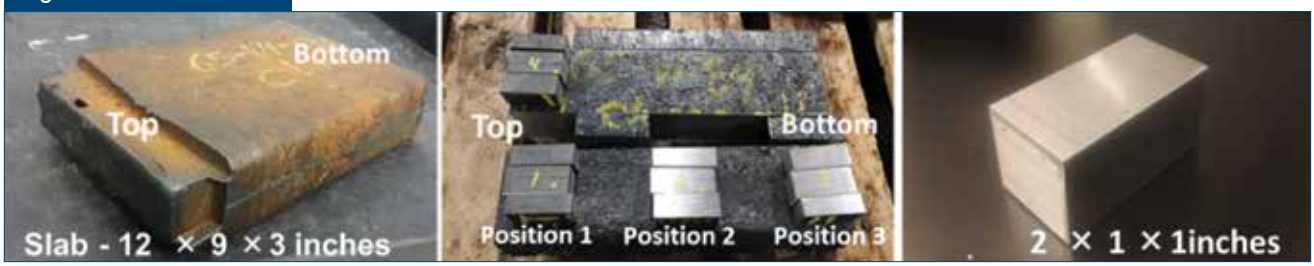

Slab sample positions sectioned for inclusion analysis. Position 1 represents the top of the slab after hot top had been sectioned out. Positions 3 is the bottom of the slab and represents inclusions at the top of the crucible.

Figure 6

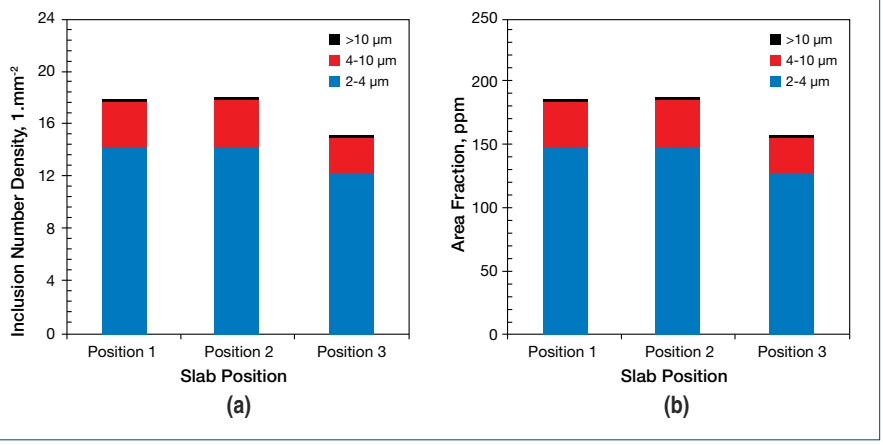

Number density and area fraction of inclusions at different positions in the slab.

Analysis of Slab Samples: For the slab samples, a 200 mm^2 area was analyzed for inclusions and the minimum analyzed inclusion size was 2 µm. To determine the best position for inclusion analysis in the slab, a preliminary experiment was conducted on the slab from heat 1. Samples for slab analysis were taken at three different positions in the slab. Fig. 5 shows the picture of the slab sample and the respective positions of sample collection. Position 1 represents the top of the slab after the hot top area was sectioned out, while positions 2 and 3 represent the middle and bottom section of the slab, respectively. The inclusions at position 3 in the slab will represent inclusions at the liquid steel surface, i.e., top of the crucible.

Fig. 6 shows the number density and area fraction of the inclusions at the different slab positions, while Fig. 7 shows the change in magnesium content and Ca/Al ratio of the inclusions. From Fig. 6, little change was noted in both the number and area fraction of the inclusions at the different slab positions. There is, however, a progressive decrease in Ca/Al ratio with increase in Mg content from position 1 to position 3, as shown in Fig. 7. Because of the little change in the number density and area fraction of the inclusions, heterogeneous dispersion of inclusions in the melt can be excluded as the cause. When calcium reacts with spinel, the magnesia content of spinel is reduced by calcium. Because of the relatively low boiling point of magnesium, magnesium vapor is produced and escapes from the liquid steel through the surface of the melt. The higher magnesium content in position 3 compared to other positions is therefore due to higher magnesium vapor at the surface of the liquid steel. Since the Ca modification reaction is occurring in the entire steel bath, it should be pointed out that the kinetics of that process and Mg removal from the steel are more favorable at position 3 than at position 1 because of lower ferro-static pressure. Steel from position 3 solidifies at the bottom of the slab where solidification is relatively fast compared to the top of the slab. For subsequent heats, inclusion analysis was done on slab samples taken from position 3.

Figure 7

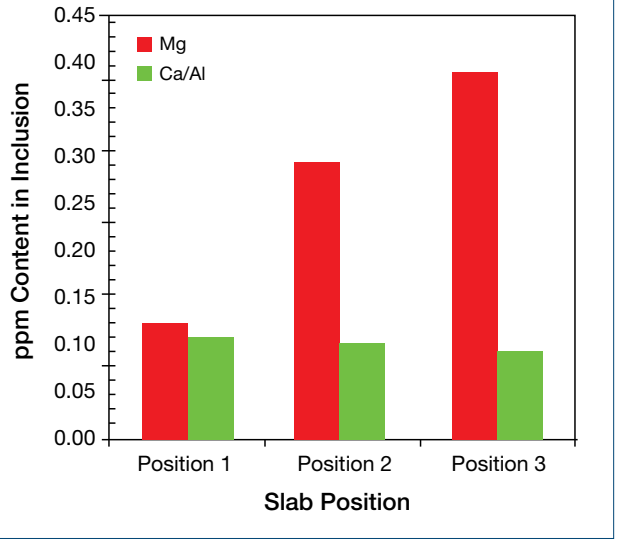

Magnesium and Ca/Al ratio of inclusions at the different slab positions. Position 3 represents inclusions at the top of the liquid steel and has the highest magnesium content in inclusions due to faster removal of magnesium vapor.

Formation of Spinel After Reoxidation — Fig. 8 shows the inclusion composition for lollipop and slab samples taken in heat 1. After aluminum deoxidation, the inclusion population consisted of alumina inclusions and transformed to both spinel and MgO inclusions after the addition of magnesium. After CaSi addition, calcium modified the spinel inclusions to both solid and liquid calcium-magnesium aluminates and CaS inclusions were also produced. The absence of pure MgO inclusions after calcium addition suggests that sample S3 was taken when the inclusions were at a transient stage. For liquid steel reoxidation, 50 ppm oxygen was added after calcium treatment. The addition of oxygen shifted the inclusion population toward the alumina-rich region and the population consisted of complex calcium-aluminate and spinel inclusions.

Figure 8

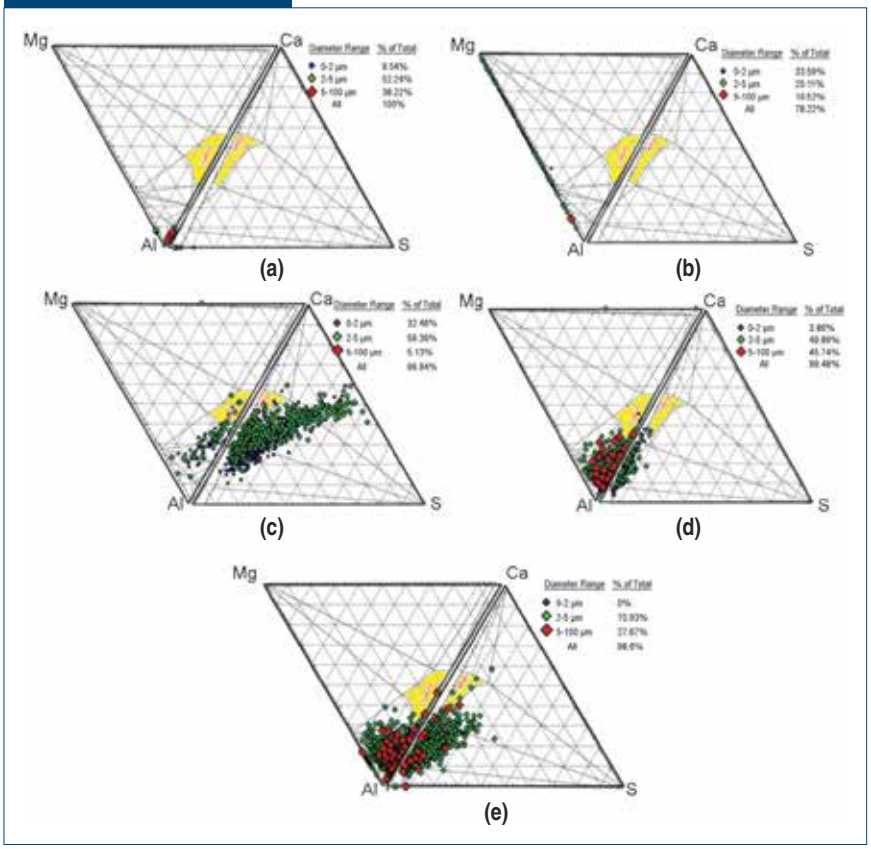

Inclusion evolution for heat 1: after deoxidation (S1) (a), after addition of magnesium (S2) (b), after calcium treatment (S3) (c), after reoxidation (S4) (d) and slab sample (e).

Figure 9

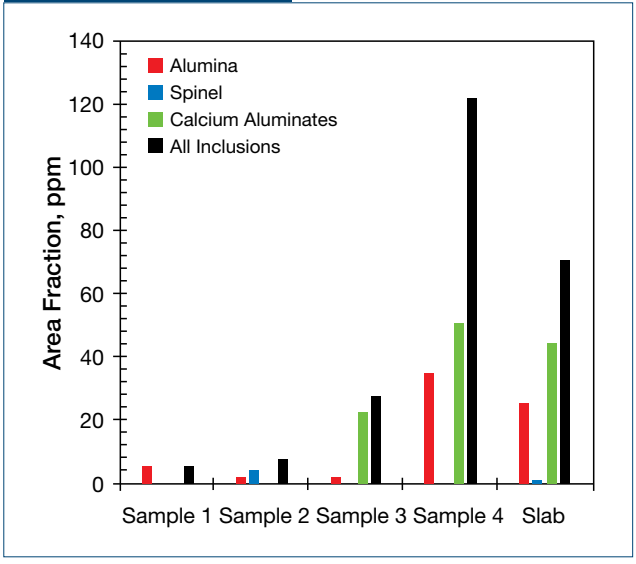

Area fraction of inclusions in samples of heat 1. A higher area fraction of spinel inclusions was observed in the slab sample (position 3) due to higher magnesium at the surface of the liquid steel.

Stoichiometric spinel inclusions were not noticed. Based on the proposed reaction mechanism for the calcium modification of spinel, magnesium goes into the solution after calcium treatment and results in the formation of spinels after liquid steel reoxidation. The lack of pure spinels in heat 1 suggests that there might not have been enough magnesium in the solution for spinel reformation. Fig. 9 shows the area fraction of the inclusions in both the liquid steel and slab sample. In the slab sample (from position 3), the presence of spinel inclusions is observed in addition to alumina and calcium aluminate inclusions. As mentioned earlier, the magnesium content at the top of the crucible is highest due to flotation of magnesium vapor and the inclusions at this position are represented by position 3 in the slab, which was used for inclusion analysis. This result, therefore, suggests that magnesium is leaving the liquid steel after calcium treatment. Chemical analysis showed a consistent Mg analysis of less than 3 ppm in samples 2, 3 and 4. Dissolved Mg, however, can be as low as 0.5 ppm, and to measure the small amounts of Mg for future experiments, a change was made to the magnesium standard used for ICP analysis and applied to heats 2 and 3.

For heats 2 and 3, the CaSi addition amount was increased from 200 g to 250 g. Also, 80 g of Mg alloy was added after calcium treatment and Fe_2O_3 addition for reoxidation to produce spinel inclusions. For heat 2, the magnesium alloy was added after the addition of Fe_2O_3, while in heat 3 magnesium alloy and Fe_2O_3 were added together. Tables 2 and 3 show the steel composition of the samples collected in heats 2 and 3, respectively. Both heats showed the total magnesium content before calcium treatment to be about 2 ppm. After the addition of Mg alloy for spinel reformation after reoxidation, the total magnesium increased by about 3 ppm. Based on mass balance calculations, 80 g Mg alloy should have produced an increase of about 20 ppm Mg. The result therefore suggests that most of the magnesium vaporized on addition and left the crucible due to the nature of the closed system in laboratory experiments.

Table 2

Chemical Composition of Samples (Heat 2)

Time (minutes)	Sample ID	Composition, wt.%				
		C	Al	S	Ca	Mg
0	Sample 1 after Al	0.041	0.08	0.006	0.0001	0.00008
5	Sample 2 after Mg alloy	0.036	0.022	0.006	0.0001	0.00017
10	Sample 3 after CaSi	0.037	0.022	0.006	0.0017	0.00017
13	Sample 4 after Fe_2O_3	0.039	0.017	0.006	0.0009	0.00008
17	Sample 5 after Mg alloy	0.037	0.018	0.006	0.0004	0.00038

Table 3

Chemical Composition of Samples (Heat 3)

Time (minutes)	Sample ID	Composition, wt.%				
		C	Al	S	Ca	Mg
0	Sample 1 after Al	0.0389	0.051	0.005	0.0001	0.00008
5	Sample 2 after Mg alloy	0.0384	0.053	0.005	0.0001	0.00012
10	Sample 3 after CaSi	0.0416	0.054	0.005	0.0029	0.00010
16	Sample 4 after Fe_2O_3 + Mg alloy	0.0404	0.051	0.005	0.0016	0.00034

Figs. 10 and 11 show the inclusion composition for samples in both heats 2 and 3 after the addition of calcium and also after reoxidation and addition of magnesium. Heat 3 had a lower oxygen content (177 ppm O) before Al addition compared to heat 2 (394 ppm O). The higher calcium and presumably low total oxygen of heat 3 resulted in the formation of large number of CaS inclusions, as shown in Fig. 10b. Fig. 12 shows the area fraction of inclusions in the liquid steel for these heats. The area fraction of the inclusions in heat 2 are about seven times higher than that observed in heat 3 due to the higher oxygen content. After reoxidation and addition of magnesium, pure spinel and MgO inclusions are observed in both heats. In heat 2, however, there is complete transformation of calcium aluminates to spinels, as observed by the disappearance of calcium aluminates in sample 5 taken after reoxidation (Fig. 10b); additionally some MgO inclusions were also noticed, indicating the possibility of intense Mg reaction in the heat. In heat 3, the simultaneous addition of both magnesium and Fe_2O_3 resulted in some unreoxidized calcium-aluminate inclusions and indicated the transient state toward complete reoxidation (Fig. 11b). The competition to modify these inclusions to spinels and MgO by the Mg alloy and Fe_2O_3 suggests that reoxidation by oxygen is a must for the production of reoxidation-type spinel inclusions.

Population Density Function

Application to Industrial Trial Samples: Lollipop samples were collected at different stages in the steelmaking process during a start-up heat at an industrial mini-mill. Samples were taken from the ladle top at the end of calcium treatment and also from the tundish at different stages of liquid steel being poured. As mentioned earlier, reoxidation

Figure 10

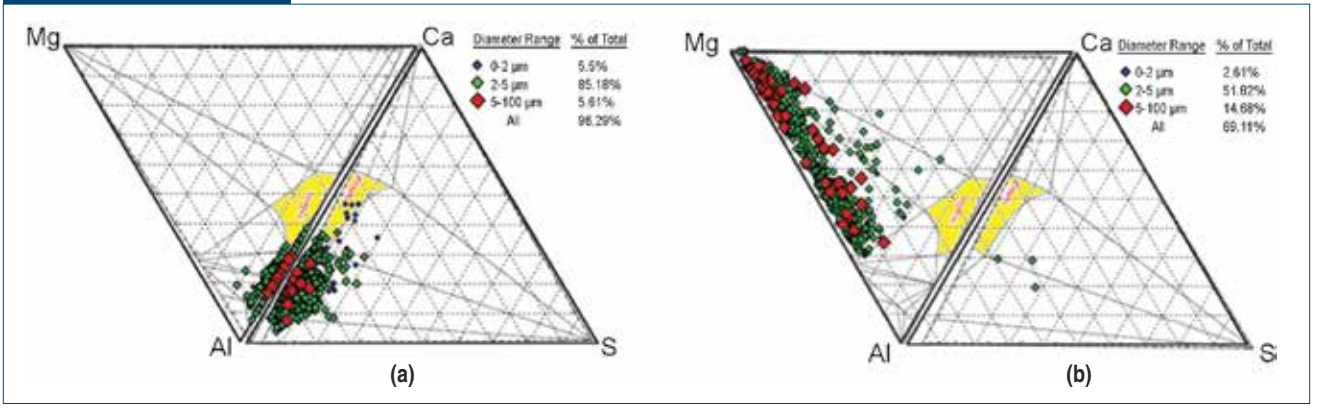

Composition of inclusions in heat 2: after calcium treatment (S3) (a) and after reoxidation and addition of magnesium (S5) (b).

Figure 11

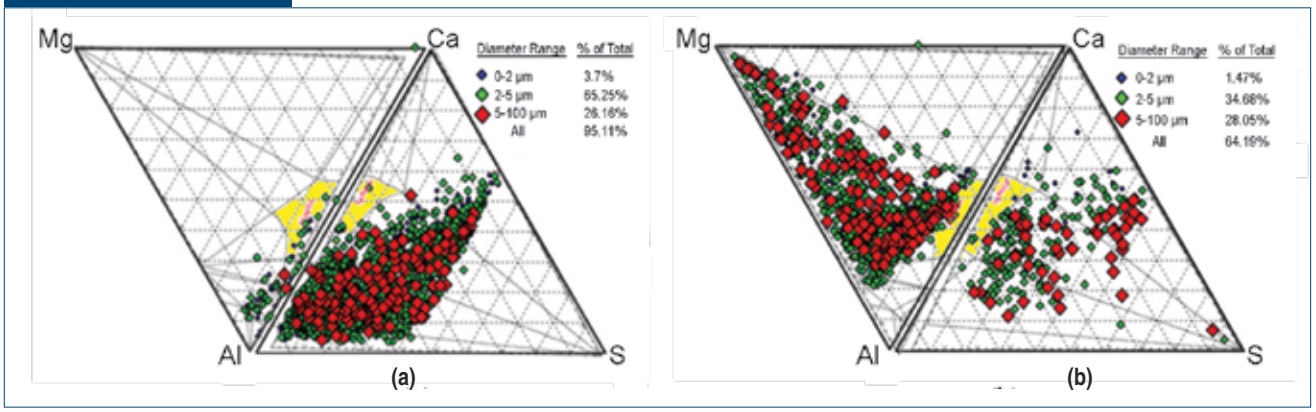

Composition of inclusions in heat 3: after calcium treatment (S3) (a) and after co-addition of magnesium and Fe_2O_3 (S4) (b).

Figure 12

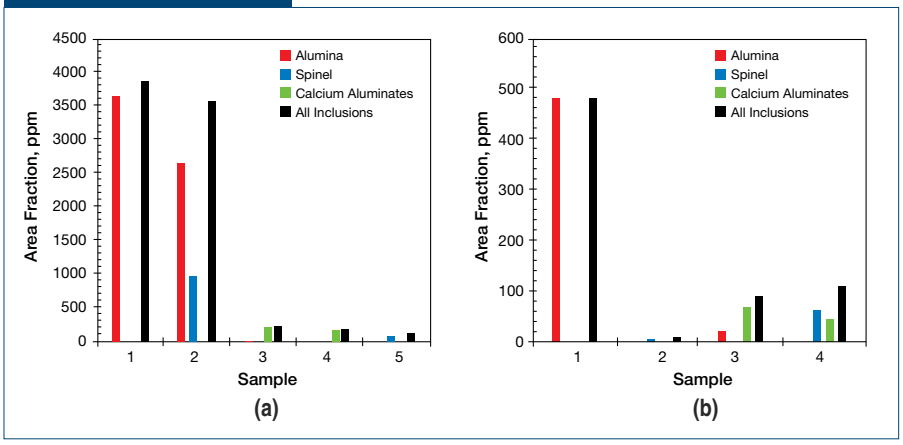

Area fraction of inclusions in heat 2 (a) and heat 3 (b). The area fraction of the inclusions in heat 2 are about seven times more than that observed in heat 3 due to the higher initial oxygen content (O) at start of the experiment in heat 2.

Table 4

Sample location

Sample No.	Steel treatment	Stage
1	After Ca addition	LMF
2	T1 (85% steel in ladle)	Tundish
3	T2 (75% steel in ladle)	
4	T3 (50% steel in ladle)	
5	T4 (10% steel in ladle)	

has been observed to occur during liquid steel transfer from the ladle to the tundish in a start-up heat because the liquid steel is totally exposed to the atmosphere with no slag covering at the start of transfer. The weight of liquid steel in the ladle was 170 tons and approximate casting duration was 45 minutes. Table 4 shows the sampling locations during this heat. The lollipop samples were sectioned, polished and analyzed for inclusions using SEM with EDS capability. Post-processing analysis was done using methodology described in Reference 10. Fig. 13 shows the inclusion composition after calcium treatment and in the tundish at initial pouring time (sample T1). During steel transfer, a shift in the inclusion population is observed toward alumina side of the ternary diagram in increasing fractions (Fig. 13) and the presence of fine alumina-rich inclusions suggests that this change resulted from reoxidation.

Fig. 14 shows the ln PDF vs. ln D (inclusion diameter) plots for the size distribution of oxide inclusions in the respective samples of the start-up heat. In LMF final sample, a linear inclusion size distribution was observed. After transfer of liquid steel from the LMF and to the tundish, the size distribution changes from linear to quadratic. This change in the shape of the inclusion distribution resulted from reoxidation. As mentioned earlier, for a start-up heat, initial liquid steel transfer into the tundish is done without slag cover and exposes the steel to atmospheric oxygen. This initial exposure to atmospheric oxygen results in reoxidation of the liquid steel. Tundish flux additions are made once a significant amount of liquid steel has been poured into the tundish, which explains the reversion of the inclusion size distribution toward a linear trend toward later stages of sampling (duration T4). The shift in shape agrees with the model proposed by Ende[1] and suggests that a linear distribution is present when the inclusions are in dynamic equilibrium with the steel, and when under active

Figure 13

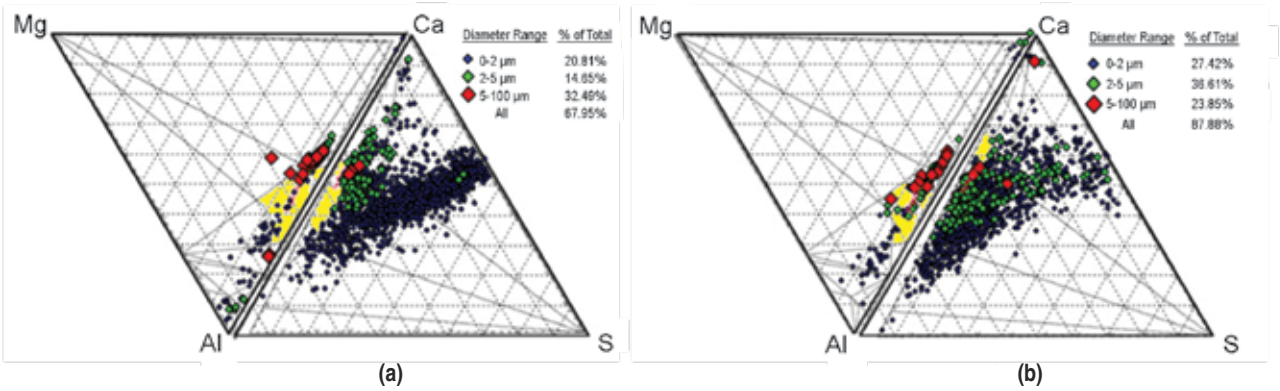

Inclusion composition at final LMF (after Ca treatment) (a) and tundish (duration T1) (b). Presence of fine alumina inclusions in the tundish is evidence of reoxidation during transfer.

Figure 14

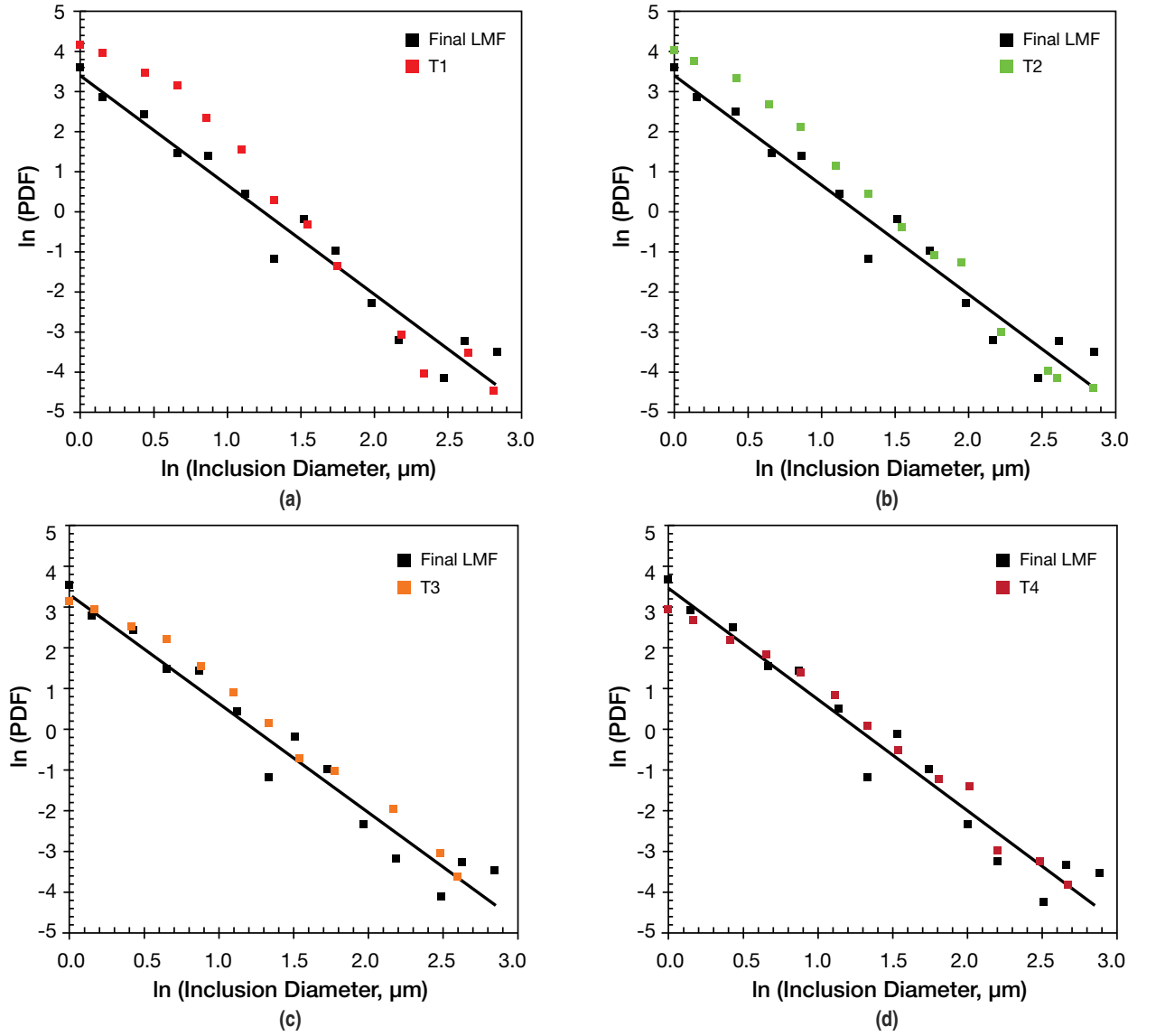

Size distribution of oxide inclusions observed in tundish samples taken from a start-up heat: positions 1 (a), 2 (b), 3 (c) and 4 (d).

Figure 15

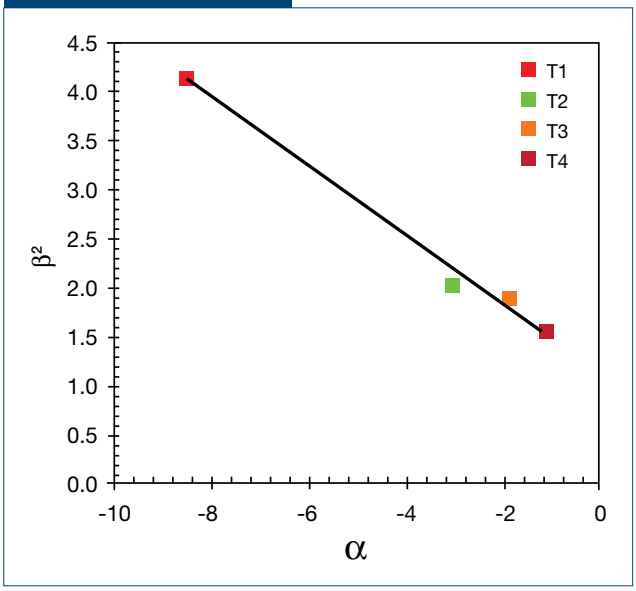

Plot of β^2 and α for samples taken from the tundish. The observed negative slope suggests the shape change resulted from Ostwald ripening.

nucleation and growth, the inclusion size distribution is quadratic. By fitting a second-degree equation to the PDF plots for the tundish samples, the shape and mean parameters (β and α) for each distribution were determined and the result is plotted in Fig. 15. This result shows a decreasing value of β^2 with increasing α and a comparison to the model by Eberl et al.[1] confirms Ostwald ripening as the major cause of the shape change in the tundish samples.

Application to Laboratory Heat Samples: The PDF method was applied to the liquid steel samples from the laboratory study to observe possible changes in the inclusion size distribution of spinel inclusions formed before and after reoxidation. Figs. 16 and 17 show the size distribution and ln PDF-ln D (inclusion diameter) plots of spinel inclusions in both heats 2 and 3, respectively. Because of the relatively higher initial oxygen content in heat 2 compared to heat 3, the high number of alumina inclusions produced after deoxidation made transformation to spinel difficult. This is seen by the observed quasi-quadratic distribution of spinel inclusions before reoxidation in heat 2. For the same time between alloy addition and sampling, a linear distribution of spinel inclusions is observed in heat 3, as shown in Fig. 17. The linear distribution for the spinel inclusions observed before reoxidation in heat 3 suggests that the inclusions were in equilibrium with the liquid steel prior to sample collection. After reoxidation, the quadratic shape is a result of nucleation and growth. About 4 minutes was given between alloy addition and sample collection, and the quadratic trends for the samples collected after reoxidation suggests that more time might have been required after reoxidation for the inclusions to attain equilibrium. Fig. 18 shows the size distribution of calcium-aluminate inclusions in heat 3 for comparison purposes only. Contrary to spinels, quadratic size distributions are observed both before and after reoxidation, suggesting that these inclusions were still undergoing reactions when the liquid steel was sampled.

In this laboratory study, the results show that the spinel inclusions observed after reoxidation are larger in size than those observed before reoxidation. The inclusion sizes and aspect ratios in both samples are summarized in Tables 5 and 6. Comparison of the size of spinel inclusions formed after reoxidation to calcium-aluminate inclusions before reoxidation shows that the spinel inclusions formed after reoxidation are similar in size to the calcium-aluminate inclusions formed after calcium treatment but before reoxidation. The larger spinel size is therefore possibly due to heterogeneous nucleation of spinel particles on the existing inclusion population and based on the thermodynamic model, suggests that spinels are formed after the calcium aluminates.

Figure 16

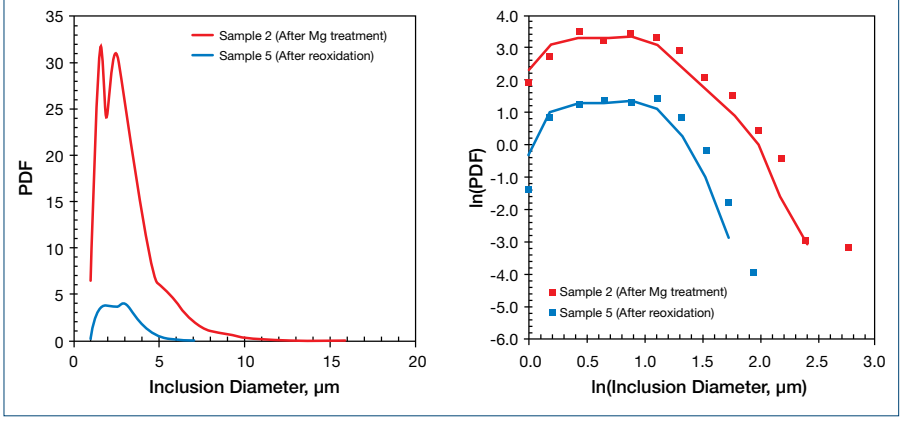

Size distribution of spinel inclusions in heat 2. Quadratic size distribution of spinel inclusions observed before reoxidation suggests that more time is required between sampling.

Summary and Conclusions

The effect of reoxidation on the formation of spinel inclusions was investigated in a laboratory study by application of the population density function (PDF). PDF was applied to study the

Figure 17

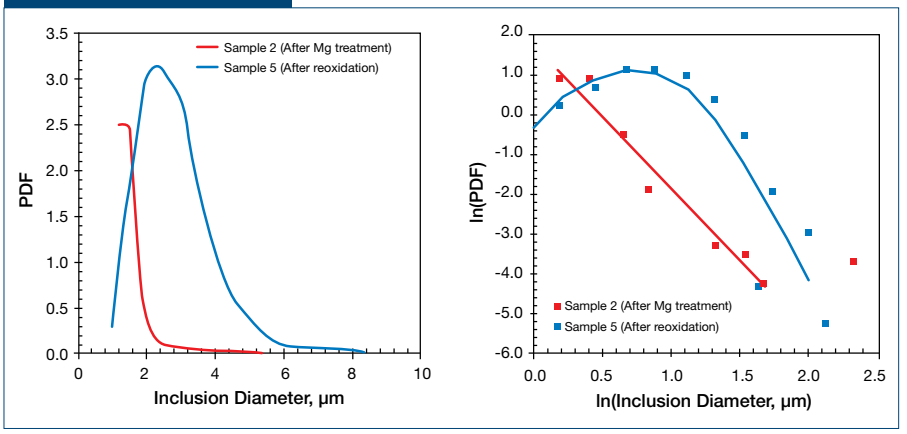

Size distribution of spinel inclusions in heat 3. Linear size distribution of spinel inclusions observed before reoxidation suggests that the inclusions were in equilibrium with the steel. After reoxidation, a quadratic distribution is observed and the spinel inclusions are larger in size.

Figure 18

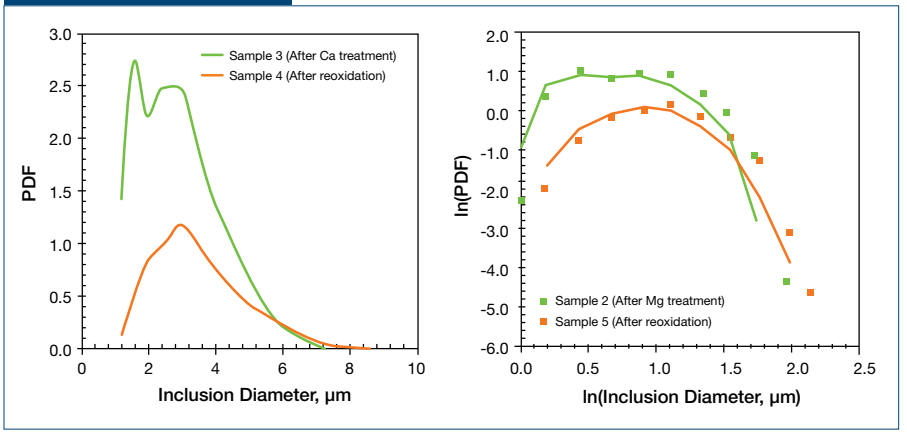

Size distribution of calcium aluminate inclusions in heat 3. Quadratic size distribution of calcium aluminate inclusions observed before and after reoxidation suggests that these inclusions where still reacting when the liquid steel was sampled. This suggests more time is required between sampling.

inclusion characteristics from industrial mini-mill and laboratory samples. The results showed that at low magnesium content in steel solution (about 1 ppm) complex calcium-magnesium aluminate inclusions are formed. Pure spinel inclusions were observed to form when the magnesium content was increased to about 4 ppm. During liquid steel processing at industrial mini-mills, MgO saturated slags are used at the LMF. These slags protect the melt from atmospheric oxygen and can also prevent escape of magnesium vapor to the atmosphere and hence keep the magnesium in the steel high enough for spinel formation at the LMF; for spinel reformation after reoxidation, both Mg and oxygen are required in the system, which are available in the tundish during casting operations.

Application of PDF to industrial mini-mill samples showed a linear distribution after calcium treatment, which transformed to quadratic distribution due to liquid steel reoxidation. Both distributions were in agreement with literature and suggest inclusion-steel dynamic equilibrium after calcium treatment and active nucleation in the tundish.

Table 5

Calcium Aluminate Inclusion Characteristics (Heat 3)

	Calcium-aluminate inclusions			
	Heat 2		Heat 3	
Process stage	Size, µm	Aspect ratio	Size, µm	Aspect ratio
Before reoxidation	2.70	1.16	2.96	1.19
After reoxidation	3.02	1.14	3.53	1.12

Table 6

Spinel Inclusion Characteristics (Heat 3)

	Calcium-aluminate inclusions			
	Heat 2		Heat 3	
Process stage	Size, µm	Aspect ratio	Size, µm	Aspect ratio
Before reoxidation	3.13	1.58	1.56	1.30
After reoxidation	2.77	1.17	2.82	1.17

Application of PDF to samples from laboratory heats showed that more time between sampling might be required for samples that showed quadratic distributions in order to attain liquid steel-inclusion dynamic equilibrium. Analysis of the size distribution of spinel inclusions from the laboratory experiments showed that after reoxidation, the mean size of spinel inclusions increased to 3 µm from about 1.5 µm before reoxidation. This increase suggests that the spinel inclusions nucleated from existing calcium aluminate inclusions.

Acknowledgments

The authors would like to give special thanks to the team at ArcelorMittal Global R&D for performing the laboratory experiments, measuring steel composition and conducting inclusion analysis; in particular, H. Pielet, B. Chukwulebe and D. White for their feedback throughout this work. The authors also acknowledge participating industrial members of the Peaslee Steel Manufacturing Research Center (PSMRC) at Missouri University of Science and Technology for providing industrial samples and financial support.

References

1. E.B. Pretorius, H.G. Oltmann and B.T. Schart, "An Overview of Steel Cleanliness from an Industry Perspective," *AISTech 2013 Conference Proceedings,* Vol. I, 2013, pp. 993–1026.
2. N. Verma, P.C. Pistorius, R.J. Fruehan, M.S. Potter, H.G. Oltmann and E.B. Pretorius, "Calcium Modification of Spinel Inclusions in Aluminum-Killed Steel: Reaction Steps," *The Minerals, Metals & Materials Society and ASM International,* Vol. 43B, 2012, pp. 830–840.
3. O. Adaba, M. Harris, R.J. O'Malley, S.N. Lekakh and V.L. Richards, "An SEM/EDS Statistical Study of the Effect of Mini-Mill Practices on the Inclusion Population in Liquid Steel," *Proc. Clean Steel 9, 9th International Conference and Exhibition on Clean Steel,* 8–10 September 2015, Budapest, Hungary, Chapter 4, Paper 5.
4. M-A. Van Ende, M. Guo, E. Zinngrebe, B. Blanpain and I-H. Jung, "Evolution of Non-Metallic Inclusions in Secondary Steelmaking: Learning From Inclusion Size Distributions," *ISIJ International,* Vol. 53, No. 11, 2013, pp. 1974–1982.
5. E. Zinngrebe, C. Van Hoek, H. Visser, A. Westendorp and I-H. Jung, "Inclusion Population Evolution in Ti-Alloyed Al-Killed Steel During Secondary Steelmaking Process," *ISIJ International,* Vol. 52, 2012, No. 1, pp. 52–61.
6. D.D. Eberl, V.A. Drits, J. Srodon, "Deducing the Growth Mechanisms for Minerals From the Shapes of Crystal Size Distributions," *American Journal of Science,* Vol. 298, 1998, pp. 499–533.
7. B.D. Marsh, "Crystal Size Distribution (CSD) in Rocks and the Kinetics and Dynamics of Crystallization I. Theory," *Contributions to Mineralogy and Petrology,* Vol. 99, 1988, pp. 277–291.
8. K.V. Cashman and J.M. Ferry, "Crystal Size Distribution (CSD) in Rocks and the Kinetics and Dynamics of Crystallization III. Metamorphic Crystallization," *Contributions to Mineralogy and Petrology,* Vol. 99, 1988, pp. 401–415.
9. M. Harris, O. Adaba, S. Lekakh, R. O'Malley and V.L. Richards, "Improved Methodology for Automated SEM/EDS Non-Metallic Inclusion Analysis of Mini-Mill and Foundry Steels," *AISTech 2015 Conference Proceedings,* Vol. II, 2015, pp. 2315–2325.
10. M.A. Van Ende, M.X. Guo, E. Zinngrebe, R. Dekkers, J. Proost, B. Blanpain and P. Wollants, "Morphology and Growth of Alumina Inclusions in Fe-Al Alloys at Low Oxygen Partial Pressure," *Iron and Steelmaking,* Vol. 36, Issue 3, 1 April 2009, pp. 201–208.
11. M.D. Higgins, "Measurement of Crystal Size Distribution," *American Mineralogist,* Vol. 85, 2000, p. 1105–1116.
12. M-D. Seo, J-W. Cho, K. Chun and S. Hyo, "Evolution of Non-Metallic Inclusions in Ultra Low Carbon Steel After Aluminum Deoxidation," *ISIJ International,* Vol. 54, No. 3, 2014, pp. 475–481.
13. B.D. Marsh, "On the Interpretation of Crystal Size Distribution in Magmatic Systems," *Journal of Petrology,* Vol. 39, 553–599. ✦

This paper was presented at AISTech 2016 — The Iron & Steel Technology Conference and Exposition, Pittsburgh, Pa., USA, and published in the Conference Proceedings.